Antioxidant and antibacterial hydroxyapatite-based biocomposite for orthopedic applications

Aditi Pandey[a], Swati Midha[b], Rajeev Kumar Sharma[a], Rita Maurya[a], Vinod Kumar Nigam[c], Sourabh Ghosh[b, *], Kantesh Balani[a, *]

[a] *Biomaterials Processing and Characterization Laboratory, Department of Materials Science and Engineering, Indian Institute of Technology Kanpur, Kanpur 208016, Uttar Pradesh, India*
[b] *Department of Textile Technology, Indian Institute of Technology Delhi, Hauz Khas, New Delhi 110016, India*
[c] *Department of Bio-Engineering, Birla Institute of Technology, Mesra, Ranchi 835 215, Jharkhand, India*

ARTICLE INFO

ABSTRACT

Post-implantation, vicinity acquired oxidative stress and bacterial infections lead to apoptosis with eventual bone-resorption and implant failure, respectively. Thus, in order to combat aforementioned complications, present research aims in utilizing antioxidant ceria (CeO_2) and antibacterial silver (Ag) reinforced hydroxyapatite (HA) composite with enhanced mechanical and cytocompatible properties. Highly dense (>90%) spark plasma sintered HA-based composites elicits enhanced elastic modulus (121–133 GPa) in comparison to that of HA. The antioxidant activity is quantified using ceria alone, wherein HA-ceria and HA-ceria-Ag pellets exhibits ~36 and 30% antioxidant activity, respectively, accrediting ceria as a scavenger of reactive oxygen species, which was corroborated with the % Ce^{3+} change quantified by X-ray photoelectron spectroscopy. The HA-Ag pellet shows antibacterial efficacy of ~61% for *E. coli* and ~53% for *S. aureus*, while a reduction of ~59% for *E. coli* and ~50% for *S. aureus* is observed for HA-ceria-2.5Ag pellet, affirming Ag reinforcement as an established bactericidal agent. The enhanced hydrophobicity on all the HA-based composites affords a high protein adsorption (24 h incubation). Further, elevated hFOB cell count (~6.7 times for HA-ceria-Ag on day 7) with filopodial extensions (60–150 μm) and matrix-like deposition reflect cell-substrate intimacy. Thus, synergistic antioxidant ceria and antibacterial Ag reinforcement with enhanced mechanical integrity can potentially serve as cytocompatible porous bone scaffolds or bioactive coatings on femoral stems.

1. Introduction

Bone injury and chain reactions mediated free radical species (reactive oxygen species, ROS) generation, is a critical factor to ponder upon. ROS affects the long-term stability of bone/implants, mediate apoptosis of osteoblasts and osteocytes, leading to osteoclastogenesis thereby favoring bone resorption [1]. ROS triggers responses like: (i) arresting cell proliferation, (ii) decreasing cell growth and/or differentiation, and (iii) promoting cell death by activating various signaling pathways [2,3]. ROS production in diseased states and aging overwhelms the antioxidant mechanisms (creating oxidative stress) of the body [4]; post-implantation, in such patients (disease, fracture and age-being the contributors), the oxidative stress secludes the material from the surrounding tissue and also leads to cytotoxicity [5]. Rodent bone resorption was facilitated by free radicals generated in vitro and in

vivo [6]. Furthermore, an in vivo study on rabbits reported that significant levels of oxidative stress are induced in the tissues surrounding a bone implant (especially, ceramic and titanium in comparison to polyethylene) [7]. Therefore, incorporating an antioxidant like ascorbic acid, vitamins, etc. may aid in accelerated healing of fractured bones/implants (scavenging ROS) and in-turn also provide a protection against osteoporosis [4,7,8].

Hydroxyapatite (HA, $Ca_{10}(PO_4)_6(OH)_2$), in the character of orthopedic implants, exhibits promising bioactivity on the ground that it shows structural and chemical similarity to human bone skeleton (Ca/P ratio 1.67) [9,10]. Notwithstanding the excellent biological property of hydroxyapatite, it possess poor mechanical strength [11] and in-order to enhance the same, a second material is used in combination/as a reinforcement, for instance carbon nanotube (CNT), silver, alumina, zirconia, etc. [12–14].

The role of rare-earth elements in bone tissue engineering has been reported in some studies, for example, the use of lanthanum oxide as a reinforcement material for HA, which showed enhancement of the microstructural and mechanical properties [15,16]. The rare earth ions are gaining popularity due to their similarity with calcium ions (calcium ion mediated signaling regulates various cellular processes like proliferation, differentiation and apoptosis) [17]. Due to the structure of cerium oxide (CeO_{2-x}) nanoparticles (NPs), the autoregenerative redox mechanism between Ce^{3+} and Ce^{4+} oxidation states is utilized as a biological trigger for designing a drug delivery system (mesoporous silica based) [18]. The role of cerium oxide nanocrystals to reduce ROS in human mesenchymal stem cells and human dermal fibroblasts exposed to H_2O_2 has been demonstrated [19,20]. Ceria NPs have now been reported to offer enzyme mimetic properties, like superoxide oxidase, oxidase and catalase; hence can be used in biomedicine [21], drug delivery [22], bioanalysis [23,24] and bio-scaffolds [25,26]. Ceria NPs are able to show ocular [27], neuronal [28], and radioprotection [29], in addition to a defense to heart from inflammatory and oxidative injury [30]. Literature reports the use of glass (lanthanide- doped; Ce/La; 2.5 wt%) in combination with HA (97.5 wt%), wherein a passable biocompatibility (improvement in cell adhesion and proliferation) was seen, indicating its potential application in bone tissue engineering [31]. Primary mouse embryonic fibroblast proliferation was stimulated by citrate-stabilized ceria NPs by decreasing intracellular ROS [32]. 3D glass foam scaffolds containing tailor made ceria NPs (synthesized in water as medium) could improve the osteoblastic differentiation of human mesenchymal stem cells by enhancing collagen formation [19,33]. A nanocomposite system composed of galantamine, ceria and HA species was found to be an effective anti-Alzheimer agent by removing hazardous ROS and helping in nerve cell repair [34]. In combination with poly (D,L-lactic-*co*-glycolic acid), ceria NPs leads to increase in elastic modulus and ultimate tensile strength, and also cardiac stem cells and mesenchymal stem cells viability with enhanced proliferation [35]. Though the precise physiological effect of cerium is still unknown, but it is understood that ceria NPs facilitates metabolism and protects tissues (as antioxidant). It has been observed that addition of 1, 5, 10 wt% of ceria to bovine-HA matrix, sintered at 1200 to 1300 °C gave rise to enhanced micro-hardness from 564 to 583 H_V, respectively, with highest compression strength ~107 MPa (for 5, 10 wt% ceria addition) [16].

Another major problem leading to implant failures is post-implant infections, majorly due to bacteria adhesion [13,36,37]. A significant decrease in bacterial counts (~65–90%) has been observed in HA and/or CNT-based composites reinforced with 2.5–10 wt% nano Ag [13,38], thus, drawing the conclusion that Ag-reinforced HA matrix can serve as potential antibacterial biocomposites (with 2.5 wt% as the most cytocompatibile, and also moderately anti-bacterial).

With respect to the aforementioned criteria, to the best of the information available, the novelty of this work resides in the fabrication of HA biocomposite, synergistically reinforced with ceria and Ag NPs, to develop composites for orthopedic applications (either as a bio-coating on metal substrates [12,39] for femoral stem [40] or as free standing porous scaffold [41]), intended to, thereby, fulfilling the following objectives: (i) antioxidant activity imparted by ceria NPs (scavenging

ROS), (ii) Ag NPs to stamp out the bacterial infections, and (iii) enhancing mechanical and cytocompatible properties with cooperative ceria NPs and Ag NPs reinforcement.

2. Materials and methods

2.1. Materials

Starting powders, Ag NPs, purity 99.95%, particle size ~65 nm, were purchased from Inframat Advanced Materials, US; ceria (CeO_2) NPs, particle size ~15–30 nm, purchased from Nanostructured & Amorphous Materials Inc., US; and ZnO NPs, purity > 99.99%, from Sigma-Aldrich, India.

2.2. Synthesis of hydroxyapatite and processing of composites

Suspension-precipitation method was used to synthesize HA powder [42]. Initially, CaO (18.6 g L^{-1}) was dispersed in distilled water, which was heated and stirred by a magnetic stirrer. Further, 0.17 M (Ca/P ratio same as HA) of H_3PO_4 was added drop wise to CaO medium, which was stirred for 3–4 h at 80 °C. In order to maintain the pH of the solution to 10, concentrated NH_4OH was then added drop wise, and the solution was stirred at 80 °C for 1 h. Then, the solution was left at room temperature for 24 h and the precipitate was collected by a filter paper, which was oven dried at 100 °C for 24 h, and crushed by an agate mortar to obtain powdered form of the material. The powders were calcined for 2 h at 800 °C and the calcined powders were further ball milled in ethanol for 16 h using agate jar and ball, with a ball-powder ratio of 4:1 at a speed of 300 r.p.m. The dried HA powder was sieved using ASTM 270 (53 μm) to achieve homogeneous particle size. Four different compositions of powder mixtures were prepared: (i) Hydroxyapatite (HA), (ii) Hydroxyapatite with 5 wt% ceria NPs (HA-5C), (iii) HA with 2.5 wt% Ag NPs (HA-2.5Ag), (iv) Hydroxyapatite with 5 wt% ceria NPs and 2.5 wt% Ag NPs (HA-5C-2.5Ag). The mixed powders were blended and homogenized in ethanol as a medium and oven dried at 80 °C. The powders were processed by spark plasma sintering (SPS, Dr. Sinter, Japan) in a cylindrical graphite die. Sintering was performed at 950 °C (ramp rate of 100 °C/min) and keeping the dwell time of 5 min with uniaxial pressure of 30 MPa in vacuum (~6 Pa) to obtain dense pellets of ~15 mm diameter and ~3 mm thickness.

2.3. Physical, phase and microstructural characterization

Archimedes' principle was used to measure the density of the pellets using distilled water as an immersion media. The theoretical and experimental density of HA based composites (CeO_2 and/or Ag reinforced) are mentioned in the Table 1.

The pellets were cloth polished using final alumina suspension (of particle size 1 μm). The phase analysis was performed with X-ray diffraction technique; XRD Rich-Seifert, 2000D diffractometer, operated at 25 kV and 15 mA with CuKα (λ = 1.541 Å) radiation scanned at scan rate of 0.5°/min, with a step size of 0.02°. The fractured surface of the

Table 1
Nomenclature and density of the hydroxyapatite-based SPS pellets.

Sample type	Nomenclature	Th. density(g/cm^3)	Archimedes density(g/cm^3)	% relative th. densification
HA	HA	3.16	3.01	95.3 ± 0.05%
HA-5CeO$_2$	HA-5C	3.25	3.02	92.9 ± 0.04%
HA-2.5Ag	HA-2.5Ag	3.21	3.11	96.9 ± 0.02%
HA-5CeO$_2$-2.5Ag	HA-5C-2.5Ag	3.31	3.12	94.3 ± 0.04%

samples was examined via Field Emission Scanning Electron Microscopy (FESEM; Nova NanoSEM 450).

2.4. Nanomechanical property evaluation

Nanoindentation of the pellets was performed using a Hysitron® TI 750-D Ubi-1 model, enabled with the Berkovich indenter tip having the radius of curvature ~150 nm with elastic modulus (E_i) of 1141 GPa and Poisson's ratio (ν_i) of 0.07 [43]. Instrument was calibrated with a standard fused silica having modulus of 69.6 GPa and hardness 9.25 GPa. For each sample, around 20 indents were made at a peak load of 2 mN with loading rate of 0.4 mN/s and holding of 2 s at peak load. Elastic modulus and hardness were calculated by using the method proposed by Oliver and Pharr [43]. An average of ten indents was taken to provide the average value.

2.5. Water contact angle measurement

The wettability of the surface plays a key role regulating protein and initial cell response, which was measured by the water contact angle [44] on sample surfaces ($n = 3$), using contact angle goniometer (Data-Physics Contact Angle System OCA). The measurement on each sample was repeated ten times.
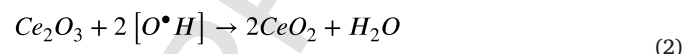
2.6. Antimicrobial test

The antibacterial activity of the samples was assessed using Gram-negative (*E. coli*; MTCC2079) and Gram-positive (*S. aureus*; MTC-C2043) bacteria. In a typical experiment, samples were polished and ultrasonicated for 15 min, autoclaved, washed with ethanol and rinsed with 1× PBS prior to seeding. In a 24 well plate, 200 μl suspension of each of the bacterial solutions (0.1 optical density) was seeded onto the samples (triplicate samples tested three times). Post-seeding, the samples were incubated for 4 h at 37 °C. The non-adhered bacterial cells were removed by thoroughly rinsing the samples with 1XPBS. Then, bacteria cultured samples were analyzed qualitatively (SEM imaging) and quantitatively (MTT assay). The attached bacterial cells were fixed with 3% glutaraldehyde, 0.1 M sodium cacodylate, and 0.1 M sucrose, for 20, 15 and 15 min, respectively. After thorough rinsing with 1XPBS, samples were dehydrated in gradient alcohol series for 10 min each and subjected to critical point drying using hexamethyldisilazane (HMDS). The samples were then sputter-coated with gold for SEM analysis (SEM; SUPRA40VP, Carl Zeiss NTS GmbH, Germany).

For determining the metabolic activity of bacterial cells, and, hence, number of viable bacterial cells, MTT assay [MTT: (3(4, 5-dimethylthiazol-2-yl)-2, 5-diphenyl tetrazolium bromide), Amresco, Life Science Research Product & Biochemicals, US] was performed. MTT: PBS in the ratio of 1:10 was added to each of bacteria cultured sample, and incubated for 2 h at 37 °C. Reacting with the viable bacterial cells, MTT forms the formazan crystals which are dissolved using dimethyl sulphoxide (DSMO) developing purple color. The absorbance of dissolved formazan crystals was determined at 570 nm wavelength, by ELISA plate reader (ultraviolet-vis BioTek, USA) [45].

2.7. Antioxidant activity determination

The antioxidant activity of ceria has been quantified observing the bacterial growth in presence of ZnO (ROS generator [42]), and ceria NPs (ROS scavenger/antioxidant). In this process, ZnO utilizes ROS to kill bacteria and on the other hand ceria NPs scavenges ROS and hence bacterial growth is increased. This difference in the bacterial viability i.e. increased bacterial growth is proportional to the ROS scavenged,

which quantifies the antioxidant activity of the ceria NPs. Therefore, a novel technique is introduced for the antioxidant activity determination. In a typical experiment, (i) Luria Broth used as growth medium supplemented with ZnO (1.47 mM or 120 μg/ml) and ceria NPs (0, 140, 280, 420, 560, 700 μM or 24, 48, 72, 96, 120 μg/ml) (ii) The ceria NPs reinforced composites (HA-5C and HA-5C-2.5Ag; $n = 3$) in LB supplemented with ZnO (1.47 mM or 120 μg/ml). As mentioned, the bioapplication of cerium oxide as a ROS scavenger/antioxidant strongly depends on the Ce^{4+}/Ce^{3+} ratio [46] where the high Ce^{3+}/Ce^{4+} ratio was beneficial, due to the Ce^{3+} free radicals scavenging action and conversion to its oxidized form, of Ce^{4+}, according to the Eq. (1) (conversion of H_2O_2 to $OH°$), 2 (oxidation of Ce^{3+} to Ce^{4+}) and 3 (reduction of Ce^{4+} to Ce^{3+}) which usually takes place in a period over ten days [47]:

$$H_2O_2 \rightarrow 2\left[O^\bullet H\right] \tag{1}$$

$$Ce_2O_3 + 2\left[O^\bullet H\right] \rightarrow 2CeO_2 + H_2O \tag{2}$$

$$2CeO_2 \rightarrow Ce_2O_3 + \frac{1}{2}O_2 \tag{3}$$

Therefore, in-order to determine the chemical states (ratio of Ce^{4+}/Ce^{3+}), X-ray photoelectron spectroscopy (XPS) was conducted on the samples (HA-5C and HA-5C-2.5Ag). For this, a PHI 5000 versa probe II (FEI Inc., Ulvac-PHI Inc., Japan) was used, operated at 25 W (15 kV) with a spatial resolution of ~10 mm (minimum probe size), 1 h scan and an energy resolution of ~0.5 eV.

2.8. Protein adsorption and cell culture

The most abundant protein found in the blood is serum albumin [48], therefore an appropriate understanding of albumin adsorption to sample surface is essential, which is evaluated by bovine serum albumin (BSA) adsorption used as a model protein. The quantitative analysis of the protein adsorption behavior was measured using standard protein adsorption protocol as per the bicinchoninic acid protein quantification assay kit (Cat. #786-570,786-571, G-biosciences). Protein concentration of 2 mg/ml was introduced on each sample ($n = 3$) in a 24 well plate, which was incubated for 24 h at 37 °C. After incubation, non-adhered proteins were removed by thorough rinsing with PBS. The concentration of adsorbed protein on the sample was evaluated at an absorbance of 540 nm, by ELISA plate reader, as per standard bicinchoninic protocol instructions. The surface roughness of the samples was measured by Optical surface profilometer (Bruker-3D optical profilometer), in-order to relate the effect of surface topography (here roughness) with adsorption behavior of the proteins and cells.

The human fetal osteoblasts (hFOBs) have been chosen for conducting in vitro tests (as it has minimal chromosomal abnormalities, immortal- non transformed cell line), for determining osteogenic responses of materials [49]. The hFOB cell line (hFOB 1.19 ATCC, CRL-11372) was purchased from Promochem, Bangalore, India. The cells were expanded in complete medium comprising of Dulbecco's modified eagles medium/nutrient mixture (F-12 Ham, 1:1 mixture Cat no. AL187A, Himedia, India) with 10% FBS (Biological Industries, Cat no. 04-121-1A) and 3 μg/ml geneticin (Cat no. 10131035, Invitrogen) at 33.5 °C in a 95% humidity and 5% CO₂. For the experiment, samples ($n = 3$) were seeded at a density 2×10^4 cells/ml in 24 well culture

plate and allowed to culture for 7 days. The protein adsorption and the MTT assay experiments were repeated three times.

For fluorescence microscopy, the samples were fixed with 3.7% formalin for 15 min, washed carefully with PBS followed by permeabilization using 0.1% TritonX100 for 10 min. Subsequently, samples were blocked with 1% bovine serum albumin for 1 h and stained with Alexa Fluor® 568 Phalloidin (Cat. No. A12380, Invitrogen) for actin staining for 1 h. Hoechst 33,342 dye (Cat. No. H3570, Invitrogen) was used for staining the nucleus. The stained cells were viewed under a confocal and multiphoton microscope system (LSM780NLO, Carl Zeiss GmbH). Cell morphology was imaged via scanning electron micrographs of hFOB-seeded samples. At 1, 3 and 7 days, cellular metabolic activity was quantified by MTT assay.

2.9. Statistical analysis

The experiments were conducted ($n = 3$) in triplicates (i.e. a total of nine measurements), unless otherwise mentioned, and the average value was calculated with the standard deviation, which was statistically analyzed by Student's *t*-test (with >95 percentage confidence level; $p < 0.05$).

3. Results and discussions

3.1. Physical, phase and microstructural analysis of spark plasma sintered hydroxyapatite-based samples

The theoretical and Archimedes' density, and the nomenclature used of HA based composites have been reported in Table 1. The XRD pattern of the sintered pellets is shown in Fig. 1. The pattern reveals the characteristic peaks of HA, confirming the occurrence of no new phase formation. The peaks for ceria are observed at 2θ value of 28.61, 47.59, and 56.48° corresponding to (111), (220), and (311) planes, and for silver at 38.23° corresponding to (111) plane. In comparison to powder, the peaks obtained in the composites are sharper with more defined reflections due to increased crystallinity, thereby suppressing some of the lower intensity peaks (making them absent after sintering).

Fig. 2a–d shows the fractured surface of the sintered pellets, which indicate an effective densification, highlighting the importance parameters chosen during spark plasma sintering technique. According to Table 1, the HA pellet shows a densification corresponding to the relative density of 95.3%, which, after addition of ceria NPs decreases to 92.9% (HA-5C), portraying highest porosity amongst the pellets. This decrement in relative density, may be attributed to the low interfacial

Fig. 1. XRD pattern of powder and composite pellets: HA, HA-5C, HA-2.5Ag, HA-5C-2.5Ag.

bonding of ceria with HA (due to the high melting temperature of ceria, 2400 °C), leading to the formation of pores in HA. The EDS mapping (Fig. 2e) of the HA-5C-2.5Ag composite shows a uniform distribution of the reinforcements Ceria and Ag.

The incorporation of silver in HA leads to an increase in the relative density as much as 96.9% (HA-2.5Ag pellet) when compared to that of HA. However, the incorporation of ceria along-with silver leads to slight decrease in relative densification (from 92.9 to 94.3%) illustrating the effect of silver in densification which may be due to the action of molten silver (at 950 °C sintering temperature), which may spread evenly, filling the pores in the HA matrix [13]. Therefore, an enhanced mechanical property is expected in composites (HA-2.5Ag and HA-5C-2.5Ag) when compared to that of HA.

3.2. Nanomechanical properties evaluation of hydroxyapatite-based SPS pellets

The nanomechanical properties of composite pellets are reported in Table 2. The Ag NPs reinforcement to HA results in an increase of the hardness (H) from 7.7 GPa (in HA) to 10.7 GPa (in HA-2.5Ag). Also, the addition of ceria alone or in combination with Ag NPs did not significantly affect the hardness of the material.

The elastic modulus (E_r) was found to be maximum for HA-2.5Ag: 132.5 GPa, followed by HA-5C-2.5Ag (128.3 GPa) and HA-5C (121.0 GPa) when compared to that of HA (99 GPa). The increased mechanical property (modulus) was due to the combined effect of composite strengthening, chemistry, and porosity of the pellets. When considering the chemistry of samples, elastic modulus of CeO_2 was found to be 190–264 GPa [50]. Besides, Afzal et al. reported that there was an enhancement in mechanical properties, hardness (by 15.5%) and modulus (4.5%) of HA-Ag composite in comparison to HA [13]. Therefore, the inherent property of reinforcements (due to the chemical composition) significantly resulted in enhanced mechanical properties (particularly E). Yet, another role by densification (porosity) of the pellets contributed significantly in the enhanced mechanical property (with increase in relative densification, porosity decreases, resulting in increased hardness and modulus). It was observed that relative densification (Table 1) decreases in the case of HA-5C and HA-5C-2.5Ag (thereby increased porosity), in comparison to HA and HA-2.5Ag (maximum relative densification), and yet an increased elastic modulus is observed relative to HA (Table 2).

It is evident from the load-displacement curve (Fig. 3) that in case of ceria and Ag NPs reinforced pellets, a smaller displacement or deformation ($h_{max} < 100$ nm) resulted in bigger fraction of elastic recovery (plasticity index, r_e of 0.50) and consequently smaller energy of dissipation (resistance to elastic recovery, r_d of 0.50) in comparison to HA pellet (r_e of 0.47, r_d of 0.53). It can be concluded that the addition of ceria and Ag NPs lead to a significant enhancement in the mechanical properties of HA, hence imparting a superior load-bearing capacity as an implant material.

3.3. Change in wettability with ceria and silver reinforcement

Table 3 summarizes the water contact angles (WCA) measured on composite pellets. It is found that the contact angle on HA-5C increased up to ~101° depicting increased hydrophobicity due to the incorporation of ceria NPs. Rare earth metal oxides (REOs) or lanthanides transition metal oxides inherently possesses hydrophobic properties because of the shielding effect (decreasing water interaction) caused due to unique electronic structure (unfilled inner, 4f orbital is shielded by an outer $5s^2p^6$ shell which forms a complete octet) [51–53]. Therefore, the measured water contact angle (~101°) for HA reinforced with ceria NPs was in accordance with previous reports [53]. When considering
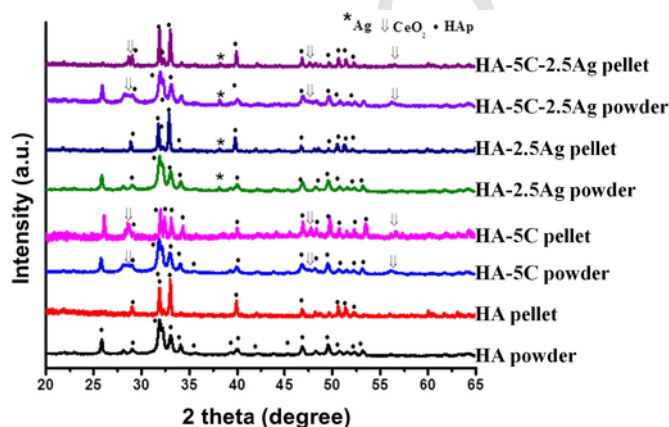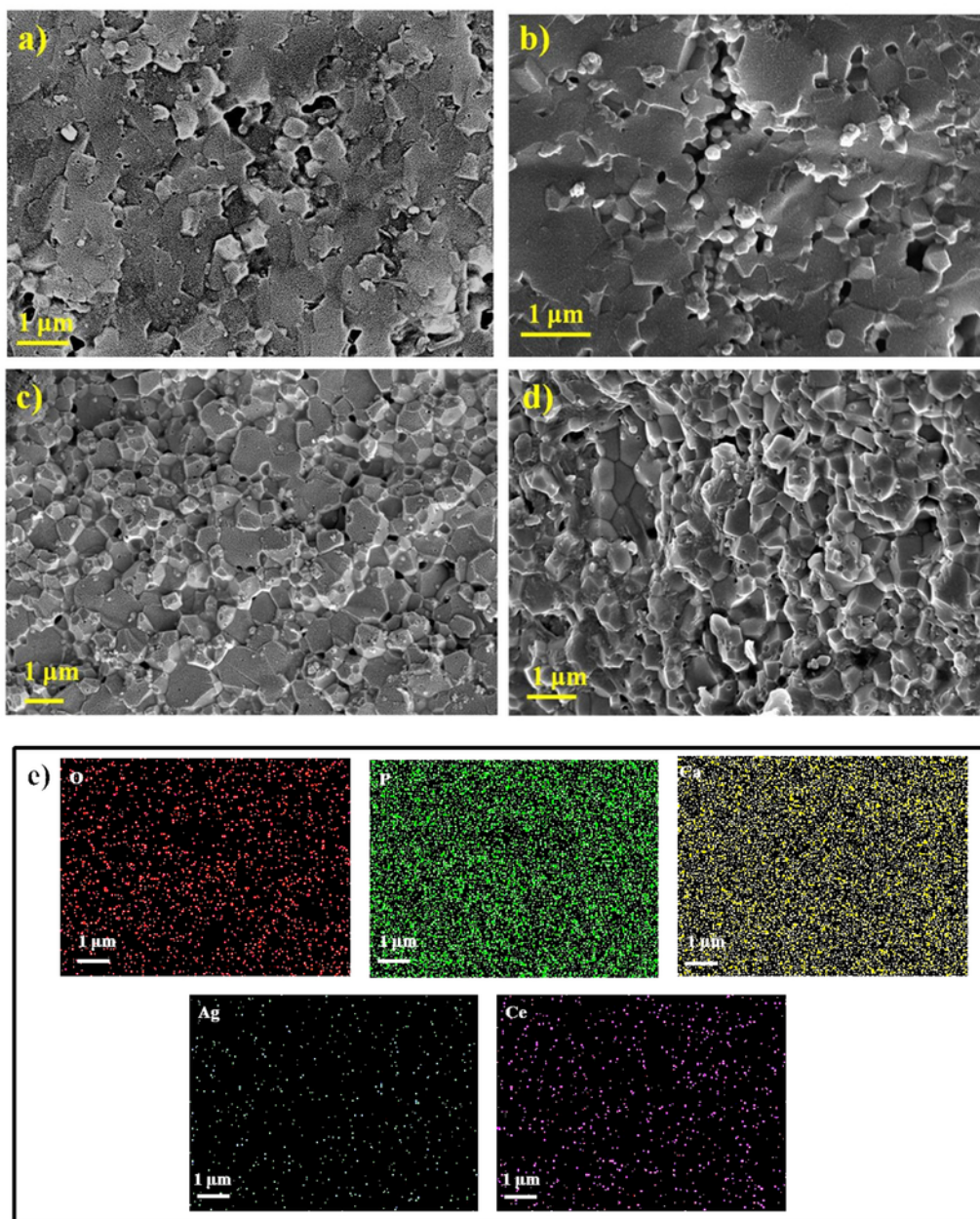
Fig. 2. FESEM images of fractured surface of a) HA, b) HA-5C, c) HA-2.5Ag, d) HA-5C-2.5Ag, and e) EDS of HA-5C-2.5Ag sintered composites.

Table 2
The nanomechanical properties of hydroxyapatite-based SPS pellets.

Sample	H (GPa)	E_r (GPa)	h_f (nm)	h_{max} (nm)	r_e ($h_{max} - h_f$)/h_{max}	r_d (h_f/h_{max})
HA	7.7±1.0	98.9±2.5	52.7	100.1	0.47	0.53
HA-5C	8.6±0.9	121.0±8.1	44.4	88.6	0.50	0.50
HA-2.5Ag	10.7±1.3	132.5±8.0	39.1	82.7	0.53	0.47
HA-5C-2.5Ag	8.3±0.6	128.3±10.1	43.0	85.6	0.50	0.50

HA-2.5Ag and HA-5C-2.5Ag surface, the contact angle is found to follow a similar trend on ceria addition, increasing from ~85° to 98°, respectively. The surface containing Ag NPs (HA-2.5Ag), was also found to be hydrophobic in comparison to HA, with the contact angle value of 85.3°, in line with the literature reported [54]. The protein and initial cell adhesion (discussed in the following sections) greatly depends
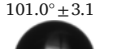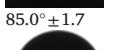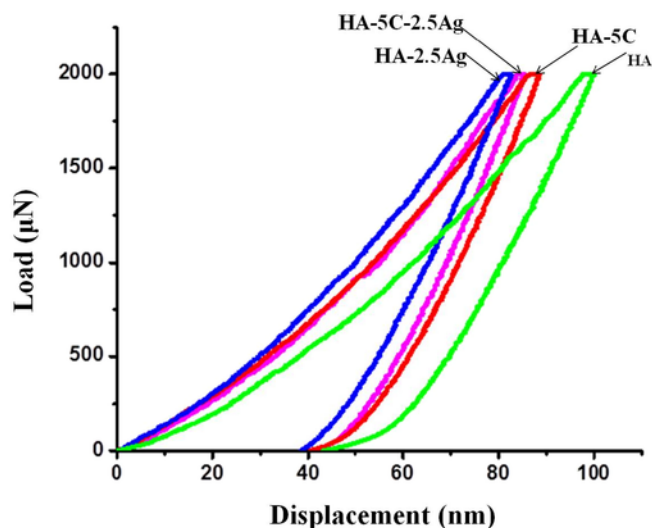
Fig. 3. Load-displacement curves of HA, HA-5C, HA-2.5Ag, HA-5C-2.5Ag sintered composites.

Table 3
Obtained values of roughness, WCA and protein adsorption on sintered pellets (* indicates significant difference of mean, *p* value <0.003 of composites in comparison to HA).

Sample type	Roughness (μm)	Contact angle (degree)	Protein adsorption (μg/mm^2)
HA	0.25±0.02	74.0°±2.0	9±0.21
HA-5C	0.33±0.04	101.0°±3.1	3.07±0.16*
HA-2.5Ag	0.33±0.03	85.0°±1.7	3.25±0.13*
HA-5C-2.5Ag	0.44±0.09	94.0°±1.7	4.34±0.12*

on wettability of the material and is expected to increase with hydrophobicity obtained in the composites [55].

3.4. Antibacterial role of silver reinforcement in hydroxyapatite-based composites

After 4h incubation, the adhesion of *E. coli* and *S. aureus* shown in Fig. 4a–d and e–h, respectively, represents the almost similar adhesion on HA (control) and HA-5C. However, samples incorporated with silver, revealed minimal bacterial density attributed to the role of silver as a bactericidal agent. The Ag ions attack the -SH groups of various enzymes, thereby, hindering protein synthesis; also the Ag ions are found to denature the bacterial DNA, leading to their bactericidal property [13].

The MTT results for *S. aureus* and *E. coli* were seen to follow a similar trend as observed in SEM images (Fig. 4i and j). The bacterial viability on HA-2.5Ag was found to be 39.33±1.76% for *E. coli* and 46.70±2.11% for *S. aureus* and on HA-5C-2.5Ag, as 41.12±1.72% for *E. coli* and 49.70±1.01% for *S. aureus*. The viability of both bacterial cultures were similar in samples without silver impregnated i.e. HA and HA-5C, albeit it was significantly lower (~40–50%) in silver-incorporated group. The results match the findings where the inert/bacterio-

static behavior of ceria NPs towards *E. coli* is reported [56,57] and a similar non-toxic nature towards *S. aureus* [58].

3.5. Antioxidant activity of reinforced ceria

The antioxidant activity of Ceria NPs is achieved in the following steps (Fig. 5a, b): (i) Bacterial growth is encouraged in presence of ZnO and in absence of ceria NPs. ZnO produces Zn^{2+} and ROS, utilizing it to kill bacteria [59], (ii) To assess the antioxidant activity of ceria NP, bacterial growth is observed both in presence of ZnO and Ceria NP, (iii) Addition of ceria NPs scavenges/kills the ROS (decreasing the total ROS), but the Zn^{2+} ions remain constant (due to similar concentration of ZnO), (iv) Therefore, an increase in the bacterial viability in presence of ceria NPs is observed, which is directly proportional to scavenged ROS by ceria NP. This, in turn, determines the antioxidant activity (AO) of ceria NPs. Using relation stated in (iv), antioxidant activity of ceria NPs has been plotted against concentration of ceria NPs as shown in Fig. 5a and b. The antioxidant activity of ~40% is achieved by addition of ~140 μM ceria NPs or in other words 2% by ~1 μg/ml of ceria, relative to that of that without ceria content. Similarly, for the composites, a significant increase in bacterial density is expected upon addition of ceria NPs. From Fig. 5c, it can be seen that in the presence of *E. coli*, the antioxidant nature (% ΔAO) of HA-5C and HA-5C-2.5Ag was found to be 36.87±5.47% and 30.67±1.67% more than that of HA and HA-2.5Ag, respectively. Along the same line, the antioxidant activity of 34.34±2.52% and 29.59±3.40% was obtained for HA-5C and HA-5C-2.5Ag pellet when compared to monolithic HA and HA-2.5Ag composite (Fig. 5d), in the presence of *S. aureus*.

The HA-5C and HA-5C-2.5Ag pellet exhibited ~36% (36±4%) and ~30% (30±3%) antioxidant activity, and the scavenging action for the free radicals was found to be almost similar in both Gram positive and Gram negative bacteria, clearly indicating the inert/bacteriostatic nature of ceria towards the bacteria. Furthermore, it can also be elucidated from Fig. 5c and d that the HA-5C-2.5Ag represents as much as ~30% antibacterial nature (represented as % Δ AB) with a simultaneous action of ROS reduction (~30%), thereby portraying a non-compromised resistance (of the construct) to bacteria in addition to antioxidant activity. This depicts the synergy between the reinforcements (ceria, for antioxidant and Ag, for antibacterial nature) in the HA matrix. The properties imparted to the HA based material would help in allowing rapid healing upon implantation and the reducing the damage caused (signaling mechanisms mediated apoptosis of osteoblasts, and activation of osteoclasts, leading to bone resorption) by the oxidative stress created in the vicinity while synergistically rendering bacterial reduction.

In order to evaluate the scavenging action of ceria exhibited by the samples, high-resolution Ce 3d XPS spectra for HA-5C and HA-5C-2.5Ag samples were recorded for the as-sintered pellets and those following ROS exposure. The peaks for Ce^{3+} and Ce^{4+} are represented in the spectra (Fig. 5e–h) and the calculated area under the peak (according to the procedure by Korsvik et al. [60]) for Ce^{3+} in the as-sintered pellets was found to be 64.4% and 59.0% in HA-5C and HA-5C-2.5Ag, respectively, which reduced to 32.3% and 33.6% after the exposure to ZnO generated ROS as shown in Table 4. This clearly corroborated the antioxidant activity (reduction in ROS/oxidation of Ce^{3+} to Ce^{4+}) obtained as 36±4% for HA-5C and 30±3% for HA-5C-2.5Ag pellet.

3.6. Protein adsorption on hydroxyapatite-based SPS pellets

From the protein adsorption data reported in Table 3, it is clear that for HA-5C surface, the adsorption was found to be 3.07 μg/mm^2, which was more than that of HA 1.13 μg/mm^2. The extent of adsorption is
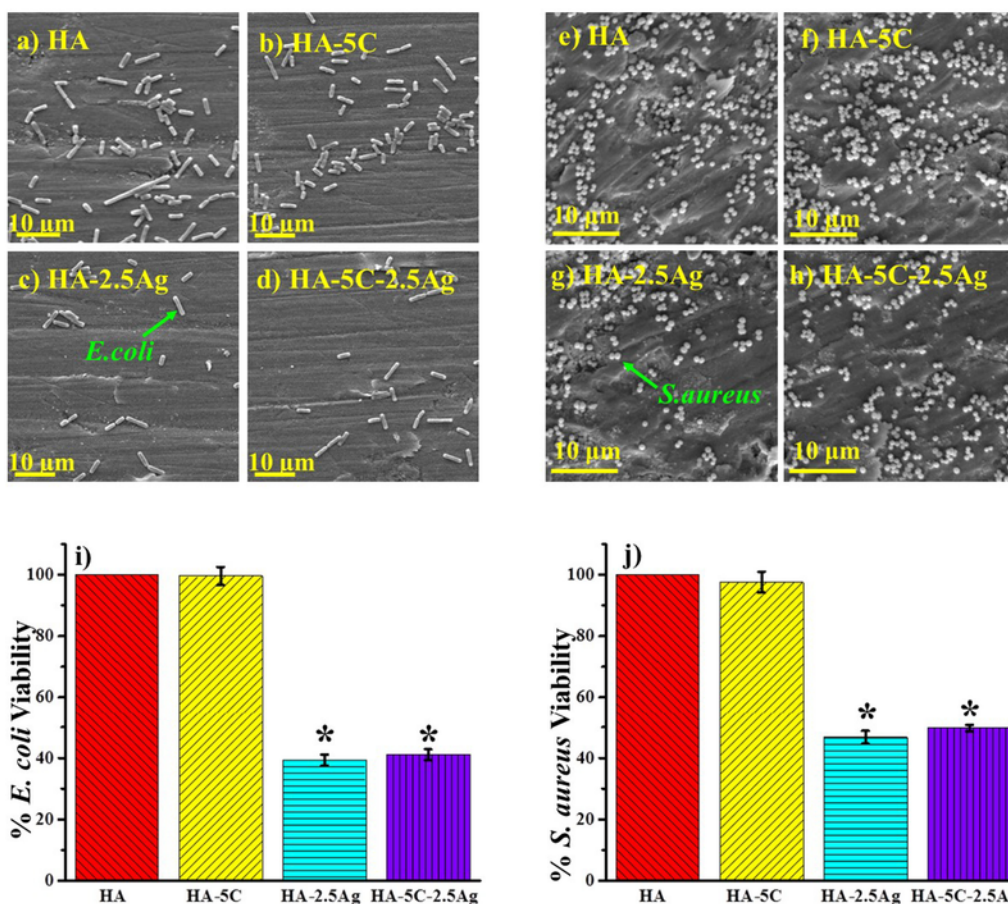
Fig. 4. Scanning electron micrographs (a–h) and quantitative estimation (i, j) of *E. coli* and *S. aureus* on HA-based sintered composites; * indicates *p* value < 0.001 of mean of HA-2.5Ag and HA-5C-2.5Ag when compared to that of HA.

significantly affected by surface properties of the material; particularly, surface charge and hydrophobicity [61]. This increase by 2.7 fold accounts for the hydrophobic surface of ceria NPs [53], which relates to its high contact angle of ~101° in HA-5C when compared to that of HA. As per the literature, it is observed that highest BSA adsorption is observed on hydrophobic surface [55]. This may explain the reason for the high adsorption of BSA (incubation time of 24 h) on the surfaces containing hydrophobic ceria NPs, as it can also be seen in the case of HA-2.5Ag pellet i.e. $3.2\,\mu g/mm^2$, when compared with HA-5C-2.5Ag pellet ($4.34\,\mu g/mm^2$), increasing by 1.34 fold, ruling out the effect of Ag NPs (due to different chemistry).

When discussing the effect of Ag NPs in protein adsorption, proteins spontaneously adsorb onto a silver coated implant surface [62,63]. The plausible mechanism for BSA adsorption onto ceria and/or Ag reinforced material surface represented in Scheme 1. The figure explains the hydrophobic effect coming into action between the BSA protein molecule and Ag/ceria NPs, and the Ag-sulphydryl complex formation. The hydrophobic interactions strengthen upon incubation period of 24 h due to protein unfolding and relaxing upon aging, leading to the surface-exposure of hydrophobic protein residues, thereby leading to more of segment-surface contacts [61]. In addition, as per the literature, the negative $\Delta G°$ values and the occurrence of thermodynamically favored reactions in the binding of the two entities, relate to hydrophobicity [48]. The BSA-silver binding may be justified by the complex (Ag-sulphydryl) formed between sulfur (from a cysteine residue of disulfide bond) and silver, as reported [64,65].

The highest contact angle (most hydrophobic) is obtained for HA-5C (Table 3), which can be a debatable concern, though. However, considering the BSA-silver complex formation and the negative Gibbs free energy change, it can be explained for the almost equal binding of the BSA to HA-2.5Ag and HA-5C surface. It may be concluded that protein adsorption is found to be maximum ($4.34\,\mu g/mm^2$) for the HA-5C-2.5Ag composite due to the cumulative properties imparted by the ceria and Ag NPs; a lag of 3.84 fold adsorbed protein is achieved for the HA pellet in comparison to that of HA-5C-2.5Ag. Therefore, an increase in the cell adhesion is expected on the composites when compared to HA surface.

3.7. Change in cell morphology upon ceria and silver reinforcement

The destined cell behavior on the substratum surface is monitored morphologically by the confocal image analysis of the actin cytoskeleton filaments. After 7 days of incubation, hFOBs were found to be prominently adhered on material surface and well distributed across the surface. Conspicuous expression of the actin filaments was evident (Fig. 6a–d). On visual examination, the number of cells observed on the surface of HA appeared relatively lesser compared to other groups. On the contrary, confluent sheath of cells was observed on the ceria and silver containing constructs (HA-5C and HA-2.5Ag), covering the underlying material surface. As seen in Fig. 6d, actin stress fibres, prominent junctions, and distinctive filopodia-like structures emerged from the growth cone edges of the cells on HA-5C-2.5Ag surface. On the HA-5C-2.5Ag surface, the filopodia-like extensions display profound lengths in the range of 60–160 μm. These extensions, apparently,
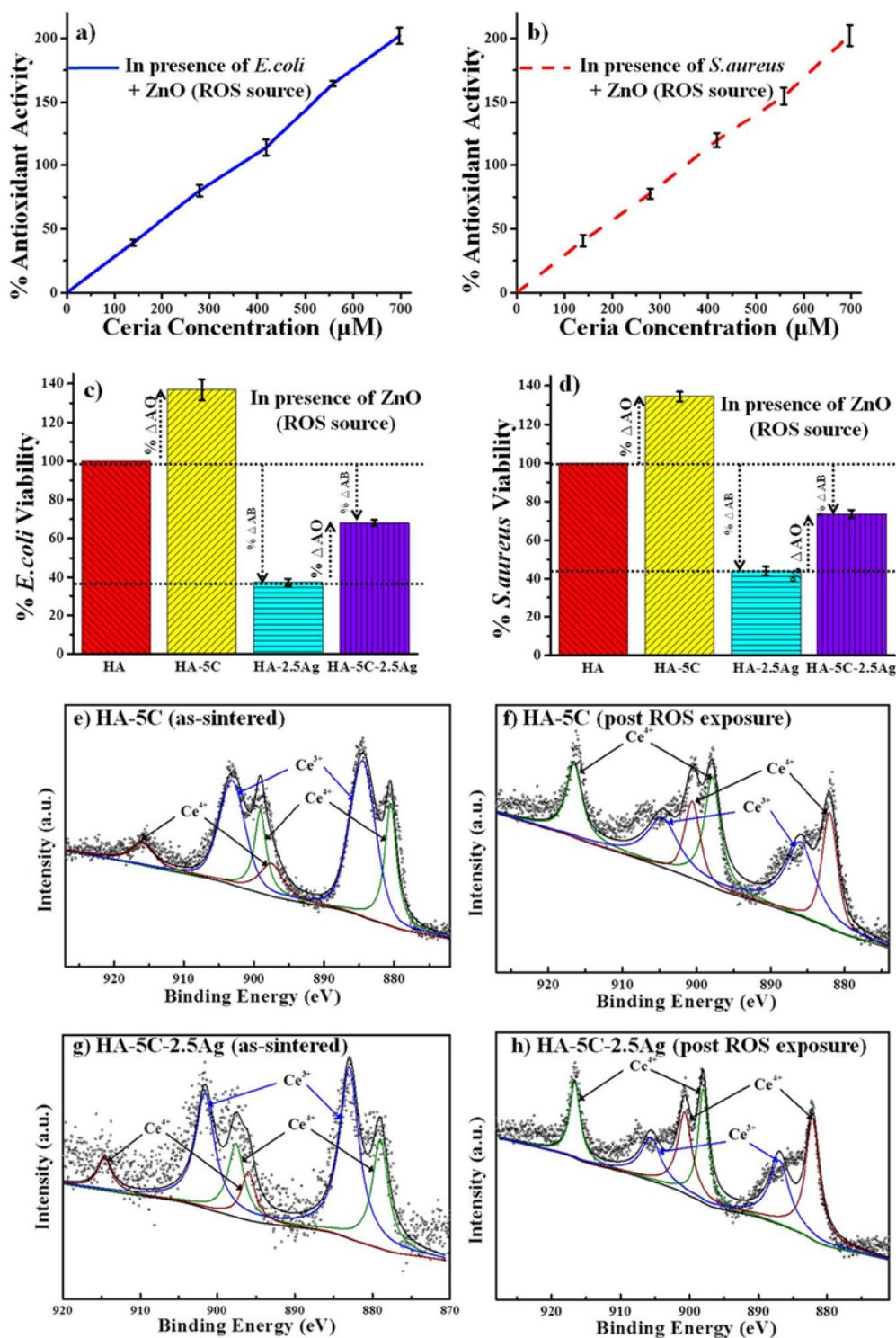
Fig. 5. Determination of antioxidant activity of ceria NPs in powder form (a, b) and in pellet: as % ΔAO (c, d) in presence of *E. coli* and *S. aureus*, with 1.47 mM ZnO as the ROS source, and XPS spectra of ceria reinforced as-sintered and post-exposure of HA-5C (e, f) and HA-5C-2.5Ag (g, h) pellets.

suggest the spreading of cell body, thereby indicating a contact intimacy with the surface. They find a role in migrating cells, wherein filopodia formation and extension probe modify extra cellular matrix (ECM) in the surrounding, thus interacting with the cells in the vicinity and facilitating cell-to-cell communications [66]. The cell-to-cell interconnectivity was very conspicuous and marked by the abundant actin

filaments, especially on the surfaces containing ceria and Ag NPs, showing a synergy of the reinforcements.

The scanning electron micrograph (Fig. 6e–h) showed irregular shaped cells across different regions of the HA surface. Moreover, cell-matrix interactions were not very prominent as cells were completely lacking any filopodial extensions. The HA-5C composite depicted high cell growth leading to cell secreted material-like deposition, whereas

Table 4
Ce^{3+} and Ce^{4+} concentration calculated from the XPS spectra.

Sample type	As-sintered		Post-ROS exposure		% change from XPS	% ROS scavenged (from experiment)
	% Ce^{3+}	% Ce^{4+}	% Ce^{3+}	% Ce^{4+}		
HA-5C	64.4	35.6	32.3	67.7	32.1	36 ± 4
HA-5C-2.5Ag	59.0	41.0	33.6	66.4	25.4	30 ± 3
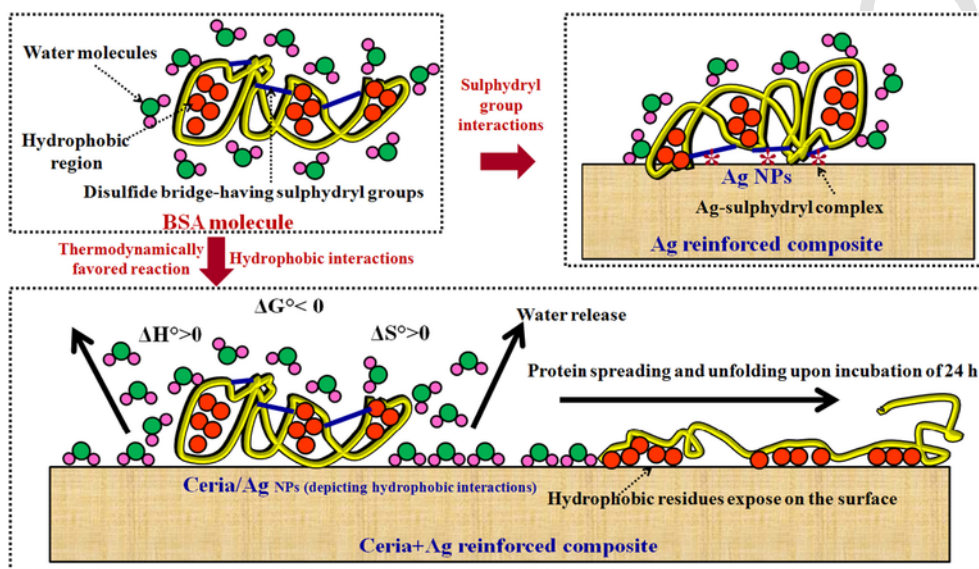
Scheme 1. Plausible mechanism of protein adsorption on ceria/Ag reinforced sintered composite.
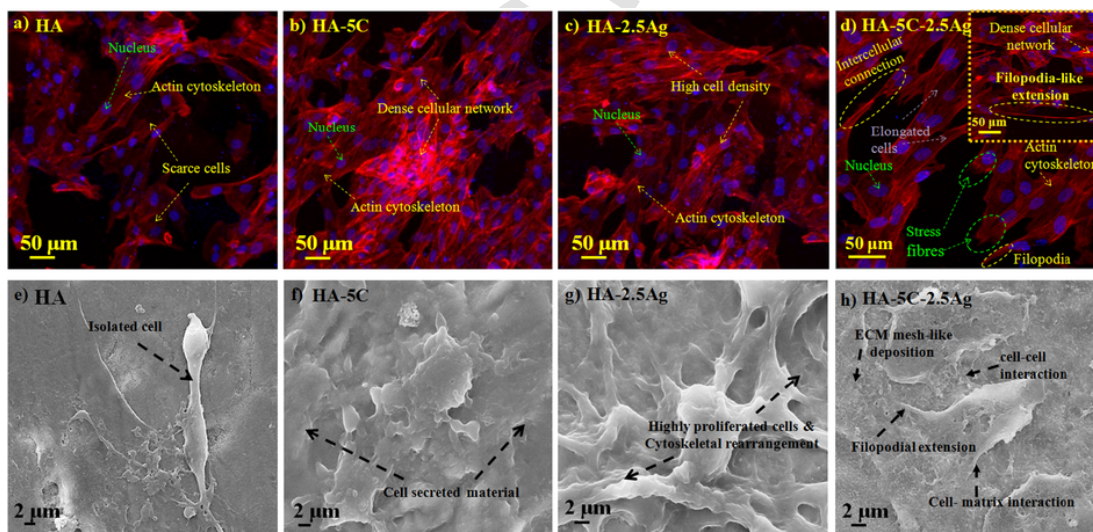

Fig. 6. Representative confocal microscopy images (a–d) and scanning electron micrographs (e–h) of cultured hFOBs on sintered composites for HA, HA-5C, HA-2.5Ag, HA-5C-2.5Ag, and HA-5C-2.5Ag, respectively.

highly proliferated cells with organized cytoskeletal arrangements was found on the HA-2.5Ag surface (Fig. 6g). The ceria and silver containing construct (HA-5C-2.5Ag) in Fig. 6h represents synergistic effect of the reinforcements, which is evident both by cell-to-cell and cell-matrix interactions, and filopodial extensions. Some regions demonstrated cell synthesized extracellular matrix mesh-like microenvironment on HA-5C-2.5Ag surface (Fig. 6h), which was not observed in the other compositions. Cytoplasmic prolongation and reorganization, and cell

synthesized matrix-like deposition can serve as a tool to study cell behavior (adhesion, proliferation, differentiation). It also serves as an indicator of physiological conditions of cell (movement and residing of cell to a tissue-specific location, forming rigorous cytoplasmic connections/ elongations in response to the environmental stimuli) [67]. Material surface appeared rough as also observed by the roughness values R_a when compared to that of HA (Table 3).

3.8. Effect of ceria and silver reinforcement on in vitro cell adhesion and metabolic activity

The quantitative analysis of the metabolic activity/viabiltiy of hFOBs on each of the substratum surface was evaluated by the MTT assay (also an indication of the obtained cell proliferation), after 1, 3 and 7 days of seeding (Fig. 7). Based on the structure-property relationship between the material surface and the cells, the plausible explanation for the adhesion and growth on biomaterials is elaborated further.

After 24 h incubation, maximum cell adhesion was observed on HA-5C-2.5Ag, followed by comparable values on HA-5C and HA-2.5Ag surfaces, with the least on HA pellet; a trend similar to that of the BSA adsorption data obtained (Table 3). The obtained cell viability values (on day 1) onto each surface defends the principle of protein adsorption (governing the cell adhesion, i.e. directly proportional to adsorbed protein), which occurred during the overnight incubation of samples in DMEM media (containing FBS protein) prior to seeding, and the interrelation instigates the process of receptor-ligand mediated cell adhesion (despite its higher hydrophobicity, now being ruled-out by the adhered protein, in turn, helping in cell adhesion). However, the process of protein adsorption occurs only up to a maximum of 48 h beyond which, the actual cell interaction without the proteins (most of them, then desorbed) takes place [68]. Cell quantification at day 3 revealed the role of material surface properties indicating cell substratum interaction. It can be elucidated that, by day 3, no significant difference was observed in hFOB metabolic activity for samples; HA, HA-2.5Ag, and HA-5C-2.5Ag, while there is a significant reduction in the cell metabolic activity obtained for HA-5C (1.5 fold lesser than day 1 HA-5C). This was most likely due to the hydrophobic ceria NPs, which were unable to attach hFOBs without prior protein adsorption.

As per the reported data, at time > 72 h falling in the post-mitotic period, the substrate surface properties may not affect cell adhesion or proliferation due to the expression of physiological activities (ECM mineralization) of cells. The time required for hFOBs to recover from hydrophobic surfaces is within 6 days of culture [69]. It can be witnessed from the data obtained on day 7 of culture period that the cell number increased considerably, especially in the hydrophobic HA-5C sample as compared to day 1 (1.4 fold) and day 3 (2.1 fold), hence discounting the effects of substrate hydrophobicity. The increase in the cell activity of all the samples with respect to HA with increasing time
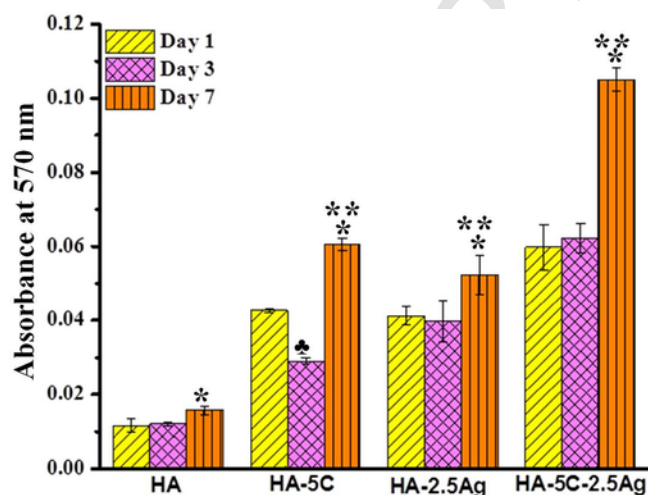

Fig. 7. hFOB metabolic activity on HA, HA-5C, HA-2.5Ag, HA-5C-2.5Ag sintered composites. (*,**, ♣ indicates *p* values of mean of cell density at day 7 composites in comparison to that of day 7 HA control: <0.001, those of day 7 in comparison to the same on day 1: <0.04 and day 3 HA-5C in comparison to that of day 1: <0.001, respectively).

confirms the cytocompatibility of the samples with osteoblast growth and activity. While, it is clear the metabolic activity of cultured hFOBs increases with time in all the samples, however, HA-5C-2.5Ag demonstrated drastically increased value (6.7 fold higher than HA on day 7), which indicates the cytocompatibility of the synergistic effects of ceria and Ag NPs.

It is believed that the as-suggested chemical similarity of Ce^{3+} to the bivalent calcium, and its capacity to bind with the calcium ions [70] result in extensive matrix deposition with 7 days as seen in Fig. 6h. This resemblance may be the primary reason responsible for its definite biological activity, and may be responsible for increasing intracellular calcium ions (ubiquitous intracellular messenger) by activation of Ca^{2+} receptor found in the membranes [71], up-regulating signaling pathways (for instance Ca^{2+}/CaM related signaling) speeding up the adhesion and proliferation of osteoblasts [72] (ceria NPs helps in metabolism, though its physiological effect is not known). It is known Ag NPs in higher concentration are toxic to cells, but at a lower concentration, are found to support cell growth [38,73], which could also help in accelerating the metabolic activity, as seen in our study.

This suggests the synergistic properties of ceria and silver aiding in an increased response towards hFOBs, observed in the form of significantly improved cell metabolic activity towards HA-5C-2.5Ag composite, along-with the formation of intracellular junctions (filopodia and its extensions) and the matrix-like deposition. It can be concluded that HA reinforcement with ceria and Ag NPs promotes cell adhesion, survival and growth which could serve as a remarkable biocompatible surface.

The various stages of the after effects of implantation (HA, HA-5C, HA-2.5Ag, HA-5C-2.5Ag implant) following a bone fracture (ROS level > Antioxidant defense: AO) is shown in Scheme 2a–d. It can be seen in the Scheme 2a that when the HA implant material (normal case) substitutes a fractured bone, the high ROS levels create a condition of oxidative stress, thereby, leading to increased bone resorption by activated osteoclasts and decreasing the bone formation. Furthermore, the bacterial attack leads to infections. The Scheme 2b shows the HA-2.5Ag implant material which decreases the bacterial attack (~50–60%) due to the action of reinforced Ag NPs, while the ROS levels do not subside. On the other hand, the HA-5C composite lead to decrement in ROS (~36%), but the bacterial infections remain, as seen in Scheme 2c. The cell response to the material increases with Ag and silver reinforcement both (Scheme 2b and c), justifying the cytocompatibility aspect. The novelty of the study is highlighted in the Scheme 2d, wherein, HA-5C-2.5Ag biocomposite depicts a perfect synergy established by the reinforcements in: (i) reducing the ROS level, ~30% due to the antioxidant activity of the ceria which would reduce bone resorption (by osteoclasts), (ii) downfall of bacterial attack by 50–60%, thereby reducing the risk of post-implant infections, due to the role of Ag, and (iii) enhanced osteoblast growth, leading to improved healing and superior bone formation due to ceria and Ag incorporation.

HA-5C-2.5Ag composite can be used either as a free-standing porous scaffold which can be utilized for internal fixation via surgical means, or as antibacterial bioactive coating on femoral stem (during fabrication of implant) for total hip-replacement. The improved and accelerated tissue healing or fracture fixation (osseointegration) aspect may be expected due to the radical scavenging by ceria.

4. Conclusions

This study aimed at the development of hydroxyapatite based composites, ceria and silver reinforced, in contemplation of encountering the oxidative stress caused in the vicinity of implants (causing apoptosis, delayed healing and implant loosening), and the bacterial fatal infections leading to implant failure. According to the as-obtained data, the incorporation of ceria and Ag NPs in HA matrix was found to be ef-
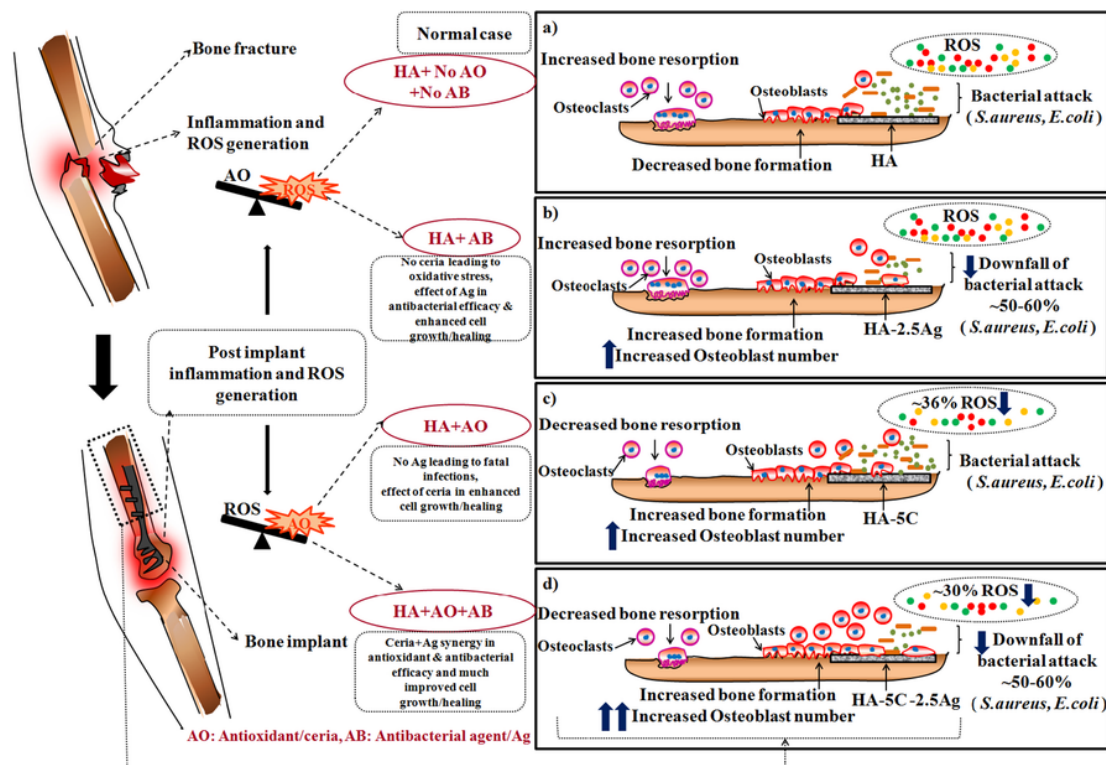
Scheme 2. Representation of after effects of HA, HA-5C, HA-2.5Ag, HA-5C-2.5Ag implants, substituting a fractured bone.

fective in reducing the ROS levels, demonstrating an antibacterial efficacy without compromising the cytocompatibiltiy. The antioxidant activity of ceria reinforced pellets, HA-5C and HA-5C-2.5Ag was found to be ~36 and 30%, respectively. The HA-Ag pellet depicted a bacterial resistance of ~61% for *E. coli* and ~53% for *S. aureus*, while HA-5C-2.5Ag showed a decrement of ~59% for *E. coli* and ~50% for *S. aureus*. The hFOB culture depicted a significant increase on all pellets by day 7, with HA-5C-2.5Ag showing highest values (6.7 times higher than that on HA). The prominent expression of actin filaments, filopodia developing into filopodia-like-extensions, and the formation of matrix like deposition (from morphological analysis) may be attributed to the synergistic effect of ceria (resemblance with calcium ions, hence mediating signaling cascades) and Ag NPs (in low concentration) for enhanced adhesion and metabolic activity supporting cytocompatibility. In addition, the composites showed enhanced mechanical property in comparison to HA (E_r ~121–133 GPa). Therefore, the HA-5C-2.5Ag biocomposite may be used as promising candidates for bone substitute (either as a free-standing porous scaffold which can be utilized for internal fixation via surgical means, or as antibacterial bioactive coating on femoral stem (during fabrication of implant) for total hip-replacement) because it provides ROS scavenging (by Ce^{3+} of ceria NPs) and promotes rapid healing (reduced oxidative stress in the implant vicinity, and enhanced osteoblast adhesion and proliferation), with antibacterial properties (of Ag NPs), enhanced mechanical properties, and improved cell growth and cytocompatibility.

Declaration

The authors declare that an Indian patent on "Antioxidant & Antibacterial Property of HA-CeO$_2$-Ag Composite for Bone Tissue Implant" was provisionally filed on November 10, 2016 (Application number: 201611038479) at the Delhi (India) patent office.

References

[1] M. Almeida, L. Han, M. Martin-Millan, C.A. O'Brien, S.C. Manolagas, Oxidative stress antagonizes Wnt signaling in osteoblast precursors by diverting betacatenin from T cell factor to forhead box 0-mediated transcription, J. Biol. Chem. 282 (2007) 27298–27305.

[2] X.C. Bai, D. Lu, A.L. Liu, Z.M. Zhang, X.M. Li, Z.P. Zou, W.S. Zeng, B.L. Cheng, S.Q. Luo, Reactive oxygen species stimulates receptor activator of NF-kappaB ligandexpression inosteoblast, J. Biol. Chem. 29 (2005) 17497–17506.

[3] S. Kousteni, FoXOs: unifying links between oxidative stress and skeletal homeostatis, Curr. Osteoporos. Rep. 9 (2011) 60–66.

[4] S.A. Sheweita, K.I. Khoshhal, Calcium metabolism and oxidative stress in bone fractures: role of antioxidants, Curr. Drug Metab. 8 (2007) 519–525.

[5] I.M. Adjei, G. Plumtom, B. Sharma, The Inflammatory Link, 1 ed., Academic Press, 2016.

[6] R. Garrett, B.F. Boyce, R.O.C. Oreffo, L. Bonewald, J. Poser, G.R. Mundy, Oxygen-derived free radicals stimulate osteoclastic bone resorption in rodent bone in vitro and in vivo, J. Clin. Invest. 85 (1990) 632–639.

[7] I. Ozmen, M. Naziroglu, R. Okutan, Comparative study of antioxidant enzymes in tissues surrounding implant in rabbits, Cell Biochem. Funct. 24 (2006) 275–281.

[8] S. Landgraeber, M. Jäger, J.J. Jacobs, N.J. Hallab, The Pathology of Orthopedic Implant Failure is Mediated by Innate Immune System Cytokines, Mediators of Inflammation, 2014, 2014, (9 pages).

[9] L.L. Hench, Bioceramics: from concept to clinic, J. Am. Ceram. Soc. 74 (1991) 1487–1510.

[10] N. Kivrak, A.C. Tas, Synthesis of calcium hydroxyapatite–tricalcium phosphate (HA–TCP) composite bioceramic powders and their sintering behavior, J. Am. Ceram. Soc. 81 (1998) 2245–2252.

[11] W. Suchanek, M. Yoshimura, Processing and properties of hydroxyapatitebased bio-materials for use as hard tissue replacement implants, J. Mater. Res. 13 (1998) 94–117.

[12] K. Balani, R. Anderson, T. Laha, M. Andara, J. Tercero, E. Crumpler, A. Agarwal, Plasma-sprayed carbon nanotube reinforced hydroxyapatite coatings and their interaction with human osteoblasts in vitro, Biomaterials 28 (2007) 618–624.

[13] M.A.F. Afzal, S. Kalmodia, P. Kesarwani, B. Basu, K. Balani, Bactericidal effect of silver-reinforced carbon nanotube and hydroxyapatite composites, J. Biomater. Appl. 27 (2013) 967–978.

[14] M.A.F. Afzal, P. Kesarwani, K.M. Reddy, S. Kalmodia, B. Basu, Functionally graded hydroxyapatite-alumina-zirconia biocomposite: synergy of toughness and biocompatibility, Mater. Sci. Eng. C 32 (2012) 1164–1173.

[15] S.S. Pazarlioglu, U. Karacayli, S. Salman, M. Yetmez, L.S. Ozyegin, S. Yilmaz, S. Agathopoulos, F.N. Oktar, Microstructure and mechanical properties of composites of bovine derived hydroxyapatite (BHA) doped with nano-powder of lanthanum oxide, Int. J. Artif. Organs 34 (2011) 700–701.

[16] O. Gunduz, C. Gode, Z. Ahmad, H. Gokce, M. Yetmez, C. Kalkandelen, Y.M. Sahin, F.N. Oktar, Preparation and evaluation of cerium oxide-bovine hydroxyapatite composites for biomedical engineering applications, J. Mech. Behav. Biomed. Mater. 35 (2014) 70–76.

[17] E.C. David, Calcium signaling, Cell 131 (2007) 1047–1058.

[18] F. Muhammad, A. Wang, W. Qi, S. Zhang, G. Zhu, Intracellular antioxidants dissolve man-made antioxidant nanoparticles: using redox vulnerability of nanoceria to develop a responsive drug delivery system, ACS Appl. Mater. Interfaces 6 (2014) 19424–19433.

[19] A.S. Karakoti, O. Tsigkou, S. Yue, P.D. Lee, M.M. Stevens, J.R. Jones, S. Seal, Rare earth oxides as nanoadditives in 3-D nanocomposite scaffolds for bone regeneration, J. Mater. Chem. 20 (2010) 8912–8919.

[20] S.S. Lee, W. Song, M. Cho, H.L. Puppala, P. Nguyen, H. Zhu, L. Segatori, V.L. Colvin, Antioxidant properties of cerium oxide nanocrystals as a function of nanocrystal diameter and surface coating, ACS Nano 7 (2013) 9693–9703.

[21] I. Celardo, J.Z. Pedersen, E. Traversa, L. Ghibelli, Pharmacological potential of cerium oxide nanoparticles, Nano 3 (2011) 1411–1420.

[22] C. Xu, Y. Lin, J. Wang, L. Wu, W. Wei, J. Ren, X. Qu, Nanoceria-triggered synergetic drug release based on CeO_2-capped mesoporous silica host-guest inter-actions and switchable enzymatic activity and cellular effects of CeO_2, Adv. Healthc. Mater. 2 (2013) 1591–1599.

[23] A. Asati, S. Santra, C. Kaittanis, S. Nath, J.M. Perez, Oxidase-like activity of polymer-coated cerium oxide nanoparticles, Angew. Chem. Int. Ed. 48 (2009) 2308–2312.

[24] C. Kaittanis, S. Santra, A. Asati, J.M. Perez, A cerium oxide nanoparticle-based device for the detection of chronic inflammation via optical and magnetic resonance imaging, Nano 4 (2012) 2117–2123.

[25] A.S. Karakoti, O. Tsigkou, S. Yue, P.D. Lee, M.M. Stevens, J.R. Jones, S. Seal, Rare earth oxides as nanoadditives in 3-D nanocomposite scaffolds for bone regeneration, J. Mater. Chem. 20 (2010) 8912–8919.

[26] C. Xu, X. Qu, Cerium oxide nanoparticle: a remarkably versatile rare earth nanomaterial for biological applications, NPG Asia Mater. 6 (2014).

[27] J. Chen, S. Patil, S. Seal, J.F. McGinnis, Rare earth nanoparticles prevent retinal degeneration induced by intracellular peroxides, Nat. Nanotechnol. 1 (2006) 142–150.

[28] B.A. Rzigalinski, K. Meehan, R.M. Davis, Y. Xu, W.C. Miles, C.A. Cohen, Radical nanomedicine, Nanomedicine 1 (2006) 399–412.

[29] R.W. Tarnuzzer, J. Colon, S. Yue, S. Seal, Vacancy engineered ceria nano-structures for protection from radiation-induced cellular damage, Nano Lett. 5 (2005) 2573–2577.

[30] J. Niu, A. Azfer, L.M. Rogers, X. Wang, P.E. Kolattukudy, Cardioprotective effects of cerium oxide nanoparticles in a transgenic murine model of cardiomyopathy, Cardiovasc. Res. 73 (2007) 549–559.

[31] J. Coelho, N.S. Hussain, P.S. Gomes, M.P. Garcia, M.A. Lopes, M.H. Fernandes, J.D. Santos, Development and characterization of lanthanides doped hydroxyapatite composites for bone tissue application, in: N.S. Hussain, J.D.d.S. Santos (Eds.), Current Trends on Glass and Ceramic Materials, Bentham Science Publishers, 2012.

[32] A.L. Popov, N.R. Popova, I.I. Selezneva, A.Y. Akkizov, V.K. Ivanov, Cerium oxide nanoparticles stimulate proliferation of primary mouse embryonic fibroblasts in vitro, Mater. Sci. Eng. C 68 (2016) 406–441.

[33] A. Karakoti, S. Singh, J.M. Dowding, S. Seal, W.T. Self, Redox-active radical scavenging nanomaterials, Chem. Soc. Rev. 39 (2010) 4422–4432.

[34] S.M.R. Wahba, A.S. Darwish, S.M. Kamal, Ceria-containing uncoated and coated hydroxyapatite-based galantamine nanocomposites for formidable treatment of Alzheimer's disease in ovariectomized albino-rat model, Mater. Sci. Eng. C 65 (2016) 151–163.

[35] C. Mandoli, F. Pagliari, S. Pagliari, G. Forte, P. Di Nardo, S. Licoccia, E. Traversa, Stem cell aligned growth induced by CeO_2 nanoparticles in PLGA scaffolds with improved bioactivity for regenerative medicine, Adv. Funct. Mater. 20 (2010) 1617–1624.

[36] J.G.E. Hendriks, J.R. Van Horn, H.C. Van Der Mei, r H.J. Bussche, Backgrounds of antibiotic-loaded bone cement and prosthesis-related infection, Biomaterials 25 (2004) 545–556.

[37] R.E. Gilbert, A.D. Carrothers, J.J. Gregory, M.J. Oakley, The St. Leger total knee replacement: a 10-year clinical and radiological assessment, Knee 16 (2009) 322–325.

[38] K. Herkendell, V.R. Shukla, A.K. Patel, K. Balani, Domination of volumetric toughening by silver nanoparticles over interfacial strengthening of carbon nanotubes in bactericidal hydroxyapatite biocomposite, Mater Sci Eng C Mater Biol Appl 34 (2014) 455–467.

[39] R.A. Surmenev, M.A. Surmeneva, A.A. Ivanova, Significance of calcium phosphate coatings for the enhancement of new bone osteogenesis - a review, Acta Biomater. 10 (2014) 557–579.

[40] R.B. Heimann, Structure, properties, and biomedical performance of osteoconductive bioceramic coatings, Surf. Coat. Technol. 233 (2013) 27–38.

[41] S. Kanhed, S. Awasthi, S. Goel, A. Pandey, R.K. Sharma, A. Upadhyay, K. Balani, Porosity distribution affecting mechanical and biological behaviour of hydroxyapatite biocomposite composites, Ceram. Int. 43 (2017) 10442–10449.

[42] N. Saha, K. Keskinbora, E. Suvaci, B. Basu, Sintering, microstructure, mechanical, and antimicrobial properties of HAp-ZnO biocomposites, J Biomed Mater Res B Appl Biomater 95 (2010) 430–440.

[43] W.C. Oliver, G.M. Pharr, Measurement of hardness and elastic modulus by instrumented indentation: advances in understanding and refinements to methodology, J. Mater. Res. 19 (2004) 3–20.

[44] Chang Hsin-I, Y. Wang, Cell Responses to Surface and Architecture of Tissue Engineering Scaffolds, InTech, 2011.

[45] S. Murab, S. Chameettachal, S. Ghosh, Establishment of an in vitro monolayer model of macular corneal distrophy, In: Laboratory Investigation, 96, Nature Publishing Group, 2016, pp. 1311–1326.

[46] H. Zhao, Y. Dong, P. Jiang, G. Wang, J. Zhang, Highly dispersed CeO_2 on TiO_2 nanotube: a synergistic nanocomposite with superior peroxidase-like activity, ACS Appl. Mater. Interfaces 7 (2015) 6451–6461.

[47] J.M. Perez, A. Asati, S. Nath, C. Kaittanis, Synthesis of biocompatible dextran-coated nanoceria with pH-dependent antioxidant properties, Small 4 (2008) 4552–4556.

[48] J. Mariam, P.M. Dongre, D.C. Kothari, Study of interaction of silver nanoparticles with bovine serum albumin using fluorescence spectroscopy, J. Fluoresc. 21 (2011) 2193–2199.

[49] M. Subramaniam, S.M. Jalal, D.J. Rickard, S.A. Harris, M.E. Bolander, T.C. Spelsberg, Further characterization of human fetal osteoblastic hFOB 1.19 and hFOB/ERaCells: bone formation in vivo and karyotype analysis using multicolor fluorescent in situ hybridization, J. Cell. Biochem. 87 (2002) 9–15.

[50] Y.L. Wang, K. Duncan, E.D. Wachsman, F. Ebrahimi, The effect of oxygen vacancy concentration on the elastic modulus of fluorite-structured oxides, Solid State Ionics 178 (2007) 53–58.

[51] K. Tsukuma, M. Shimada, Strength, fracture toughness and Vickers hardness of CeO_2 stabilized tetragonal ZrO_2 polycrystals, J. Mater. Sci. 20 (1985) 1178–1184.

[52] N. Giovambattista, P.G. Debenedetti, P.J. Rossky, Effect of surface polarity on water contact angle and interfacial hydration structure, J. Phys. Chem. B 111 (2007) 9581–9587.

[53] A. Gisele, R. Dhiman, K. Hyuk-Min, A.T. Paxton, K.K. Varanasi, Hydrophobicity of rare-earth oxide ceramics, Nat. Mater. 12 (4) (2013) 315–320.

[54] K.C. Pratik, A. Nammari, T.S. Ashton, I.M. Adjei, Saturated pool boiling heat transfer from vertically oriented silicon surfaces modified with foam-like hexagonal boron nitride nanomaterials, Int. J. Heat Mass Transf. 95 (2016) 964–971.

[55] M. Tanaka, T. Motomura, M. Kawada, T. Anzai, Y. Kasori, T. Shiroya, K. Shimura, M. Onishi, A. Mochizuki, Blood compatible aspects of poly(2-methoxyethylacrylate) (PMEA)-relationship between protein adsorption and platelet adhesion on PMEA surface, Biomaterials 21 (2000) 1471–1481.

[56] A. Thill, O.L. Zeyons, O. Spalla, F. Chauvat, J.M. Rose, M.L. Auffan, A.M. Flank, Cytotoxicity of CeO_2 nanoparticles for Escherichia coli. Physico-chemical insight of the cytotoxicity mechanism, Environ. Sci. Technol. 40 (2006) 6151–6156.

[57] J. Gagnon, M.J.D. Clift, D. Vanhecke, I.E. Widnersson, S.-L. Abram, A. Petri-Fink, R.A. Caruso, B. Rothen-Rutishauser, K.M. Fromm, Synthesis, characterization, antibacterial activity and cytotoxicity of hollow TiO_2-coated CeO_2 nanocontainers encapsulating silver nanoparticles for controlled silver release, J. Mater. Chem. B 4 (2016) 1166–1174.

[58] T.N. Ravishankar, T. Ramakrishnappa, G. Nagaraju, H. Rajanaika, Synthesis and characterization of CeO_2 nanoparticles via solution combustion method for photocatalytic and antibacterial activity studies, Chem. Open 4 (2015) 146–154.

[59] R.K. Sharma, M. Agarwal, K. Balani, Effect of ZnO morphology on affecting bactericidal property of ultrahigh molecular weight polyethylene biocomposite, Mater. Sci. Eng. C 62 (2016) 843–851.

[60] C. Korsvik, S. Patil, S. Seal, W.T. Self, Superoxide dismutase mimetic properties exhibited by vacancy engineered ceria nanoparticles, Chem. Commun. (10) (2007) 1056–1058.

[61] C.F. Wertz, M.M. Santore, Effect of surface hydrophobicity on adsorption and relaxation kinetics of albumin and fibrinogen:single-species and competitive behavior, Langmuir 17 (2001) 3006–3016.

[62] A. Ravindran, A. Singh, A.M. Raichur, N. Chandrasekaran, A. Mukherjee, Studies on interaction of colloidal Ag nanoparticles with Bovine Serum Albumin (BSA), Colloids Surf. B: Biointerfaces 76 (2010) 32–37.

[63] W. Norde, My voyage of discovery to proteins in flatland …and beyond, Colloids Surf. B: Biointerfaces 61 (2008) 1–9.

[64] D.C. Carter, J.X. Ho, Structure of serum albumin, Adv. Protein Chem. 45 (1994) 153–203.

[65] E. Podstawka, Y. Ozaki, L.M. Proniewicz, Adsorption of S-S containing proteins on a colloidal silver surface studied by surface-enhanced Raman spectroscopy, Appl. Spectrosc. 58 (2004) 1147–1156.

[66] C.A. Heckman, H.K. Plummer, Filopodia as sensors, Cell. Signal. 25 (2013) 2298–2311.

[67] Shih-Ping Yang, Hsiang-Sheng Wen, Tzer-Min Lee, Truan-Sheng Lui, Cell response on the biomimetic scaffold of silicon nano- and micro-topography, J. Mater. Chem. B 4 (2016) 1891–1897.

[68] S.K. Swain, D. Sarkar, Study of BSA protein adsorption/release on hydroxyapatite nanoparticles, Appl. Surf. Sci. 286 (2013) 99–103.

[69] X. Liu, J.Y. Lim, H.J. Donahue, R. Dhurjati, A.M. Mastro, E.A. Vogler, Influence of substratum surface chemistry/energy and topography on the human fetal osteoblastic cell line hFOB 1.19: phenotypic and genotypic responses observed in vitro, Biomaterials 28 (2007) 4535–4550.

[70] J. Jowsey, R.E. Rowland, J.H. Marshall, The deposition of the rare earths in bone, Radiat. Res. 8 (1958) 490–501.

[71] D. Riccardi, B. Finney, W. Wilkinson, P. Kemp, Novel regulatory aspects of the extracellular Ca^{2+}-sensing receptor, CaR, Pflugers Arch. - Eur. J. Physiol. 458 (2009) 1007–1022.

[72] M. Zayzafoon, Calcium/calmodulin signaling controls osteoblast growth and differentiation, J. Cell. Biochem. 97 (2006) 56–70.

[73] C. Shi, J. Gao, M. Wang, Y. Shao, L. Wang, D. Wang, Y. Zhu, Functional hydroxyapatite bioceramics with excellent osteoconductivity and stern-interface induced antibacterial ability, Biomater. Sci. 4 (2016) 699–710.